JOURNAL OF MATERIALS SCIENCE **34** (1999) 655–666

Atomistic simulation of grain boundary sliding and migration

N. CHANDRA, P. DANG
Department of Mechanical Engineering, College of Engineering, Florida A&M University, Florida State University, Tallahassee, FL 32310, USA
E-mail: me@eng.fsu.edu

Interatomic potentials using Embedded Atom Method (EAM) are used in conjunction with molecular statics and dynamics calculations to study the sliding and migration of [1 1 0] symmetric tilt grain boundaries (STGB) in aluminum, under both applied displacement and force conditions. For equilibrium grain boundaries (without applied displacements and forces), three low energy configurations (corresponding to three twin structures) are found in the [1 1 0] STGB structures when grain boundary energies at 0 K are computed as a function of grain misorientation angle. "Pure" grain boundary sliding (GBS) without migration is simulated by applying external displacement. When forces are applied, the energy barriers are reduced consequent to the fact that grain boundary sliding of STGB is always coupled with migration. The propensity for "pure" GBS is evaluated by computing the energy associated with incremental equilibrium configurations during the sliding process and compared to the case when sliding is accompanied by migration. The magnitude of the energy barriers is found to be much higher in "pure" GBS than when migration accompanies sliding. Relations between the applied force, internal stress field, and displacement field are established and the role of grain boundary structure on the deformation process are examined. It is found that the GBS displacement is proportional to applied force, GB energy, and time.

1. Introduction

Despite the important role of grain boundaries (GB) in influencing materials properties, such as superplasticity [1], our knowledge of how boundaries actually move at the microscopic level is limited. Much of the difficulty is due to the lack of a suitable means of observing the dynamical process (such as sliding and migration) with sufficient spatial and time resolution. One approach that has provided atomic-level insights of GB in metals is atomistic simulations. As an effective alternative, atomistic simulations are being used increasingly due to the availability of atomistic models and highly powerful computers. Although considerable work has been done in recent years to study the equilibrium structures of grain boundaries using atomistic simulations [2–15], only very limited research has focused on the atomistic simulation of grain boundary sliding (GBS) and migration. Yip and coworkers [16–18] studied grain boundary migration and sliding due to high temperature effect using pair-like potentials. They observed that both migration and sliding occurred purely from the effects of elevated temperatures. In general, the driving force for grain boundary movement is the internal strain and stress field [10]. Unfortunately, there are very few studies devoted to grain boundary mobility under applied strains or stresses at atomic level. Very recently Molteni *et al.* [19] conducted an *ab initio* simulation of grain boundary sliding in germanium in a quasi-static way by applying constant strain increment to one crystal of the bicrystal boundaries. The problem with applied strain instead of forces, as will be evident in the present work, is that the migration process is inhibited, altering the kinetic of the deformation process. Such a preconstrained process experiences a much larger energy barrier than a coupled sliding and migration process, which occurs naturally.

This paper's main purpose is to explain the mechanics of deformation of grain boundaries at the atomic level. In order to achieve this, first the structure and energy of the STGB of aluminum was studied. Based on the equilibrium structure, displacements and forces on one of the grains to simulate grain boundary deformation (sliding and migration) were applied. The paper is organized as follows. In section 2, the atomistic simulation methods and the interatomic potentials are first introduced. The equilibrium structure and energy of 17 [1 1 0] tilt grain boundaries in aluminum are then studied using molecular statics simulations and EAM potential functions. These boundaries were described by coincident site lattice (CSL) with misorientation angles range from 0 to 180 degree. In section 3, based on the equilibrium GB structures obtained in section 2, grain boundary mobility (sliding and migration) is then simulated under both applied displacement and applied force conditions. The mechanics (stress, displacement, and energetic fields) associated with applied

displacement and applied stress are examined to elucidate the importance of coupled sliding and migration process.

2. Equilibrium grain boundary structures and energies

Molecular statics and molecular dynamics are used in performing atomistic simulations. Molecular statics is used in determining the equilibrium positions of atoms in a crystal, by minimizing the total energy of the crystal at 0 K. Molecular dynamics is used to study the time-related phenomena for crystals subjected to external forces. A molecular dynamics/statics code (DYNAMO program) developed at the Sandia National Laboratory, Livermore, [21] incorporating the EAM model has been used in the simulation work. It has been proven that EAM potentials are more reliable in representing atomic interactions in metallic systems [11–15] than in traditional pair potentials. The main limitation of the pair potential models is that they fail to take into account the metallic bonds (i.e. coordinate-dependent or many body interactions), while EAM potentials include in an implicit way the many-body effects. The analytical EAM functions developed by Oh and Johnson [20] will be adopted in this work.

Since GBS and GB migration are the main focus of this work, grain boundaries are modeled as planar bicrystalline high-angle structures specified by coincident site lattice (CSL) models. High-angle grain boundaries (misorientation angle $\theta > 15^\circ$) are associated with higher grain boundary energy and are generally thought to promote GBS [1]. CSL grain boundaries are found to occur naturally in all polycrystalline materials, and their frequency of occurrence is strongly dependent on the processing history [22]. As the consequence of the CSL model, the lowest-energy grain boundary structure for a given misorientation (characterized by Σ) is postulated to be the symmetrical configuration. Fig. 1 illustrates the designations of symmetric tilt grain boundaries (STGB) used throughout this work. In this figure, the rotation axis [uvw] is perpendicular to the plane of the paper (z-direction), consequently, the grain boundary plane (h k l) is x-y plane with y-direction aligned to the grain boundary normal; and the misorientation angle θ is computed from the two [0 0 1] directions of each of the bicrystals. Grain boundaries are designated as [u v w] Σ N (h k l), thus the grain boundary shown in Fig. 1 describes [1 1 0] Σ3(111) tilt boundary.

In this work, 17 tilt [1 1 0] CSL boundaries: $\Sigma3(1\bar{1}1)$, $\Sigma3(1\,1\,2)$, $\Sigma9(2\,2\,1)$, $\Sigma9(1\,1\,4)$, $\Sigma11(1\,1\,3)$, $\Sigma11(3\,3\,2)$, $\Sigma17(3\,3\,4)$, $\Sigma19(3\,3\,1)$, $\Sigma27(1\,1\,5)$, $\Sigma27(5\,5\,2)$, $\Sigma33(2\,2\,5)$, $\Sigma33(4\,4\,1)$, $\Sigma33(1\,1\,8)$, $\Sigma41(4\,4\,3)$, $\Sigma43(5\,5\,6)$, $\Sigma43(3\,3\,5)$, and $\Sigma51(5\,5\,1)$ were examined. For each of the CSL boundaries, the computational crystal was generated based on the orientation of a given grain and on the symmetry between that and the adjacent grain across the boundary plane. Due to the fact that multiple energy minima may exist with very similar energies and very different atomic structures [6], it may be necessary to obtain lower-energy states by removing (or adding) atoms from the boundary plane during construction of the initial unrelaxed structures. Because grain boundaries are extended defects in two dimensions, but inhomogeneous in the direction normal to the grain boundary plane, it is usual to construct a computational crystal that is periodic only in the 2-D plane of the interface (x- and z-directions in this work). In the grain boundary normal direction (y-direction), free-surface boundary conditions are imposed. Consequently, the crystals are designed to be large enough in the y-direction to remove the free surface effects on the grain boundary structure. The computational crystals used in this work contain about five-thousand atoms.

Fig. 2 shows the final equilibrium structures of selected grain boundaries obtained using molecular statics simulations. It should be noted that for convenience only a portion of the whole computational crystal close to the grain boundary is shown. The open and filled circles represent atoms in two adjacent (1 1 0) atomic

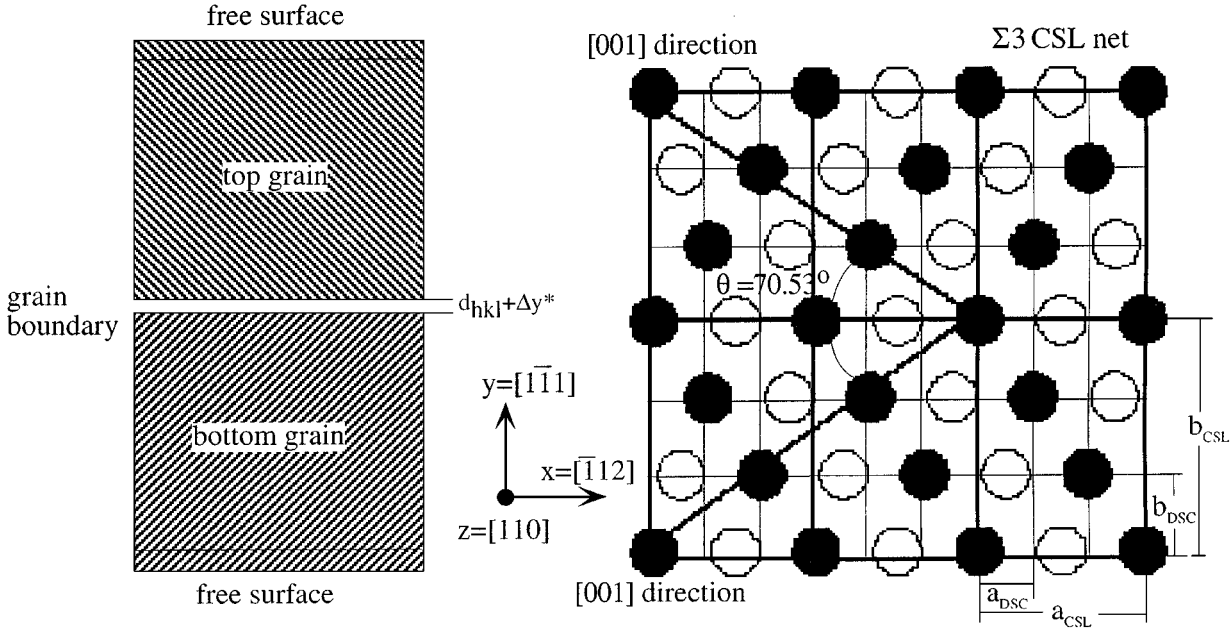

Figure 1 Schematic of the construction and notation of CSL/DSL tilt grain boundaries.

TABLE I Grain boundary energy (E_{gb}) and local displacement (Δy^*) of selected equilibrium GB structures

GB(CSL)	$\Sigma 3$ $(1\bar{1}1)$	$\Sigma 3$ $(1\,\bar{1}\,2)$	$\Sigma 9$ $(2\,\bar{2}\,1)$	$\Sigma 9$ $(1\,\bar{1}\,4)$	$\Sigma 11$ $(1\,\bar{1}\,3)$	$\Sigma 11$ $(3\,\bar{3}\,2)$	$\Sigma 33$ $(2\,\bar{2}\,5)$	$\Sigma 43$ $(3\,\bar{3}\,5)$
E_{gb} (eV/Å^2 $\times 10^{-2}$)	0.024	2.03	2.69	2.18	0.91	2.59	2.34	2.62
Δy^*(Å)	0.004	0.523	0.699	0.432	0.126	0.961	0.150	0.191

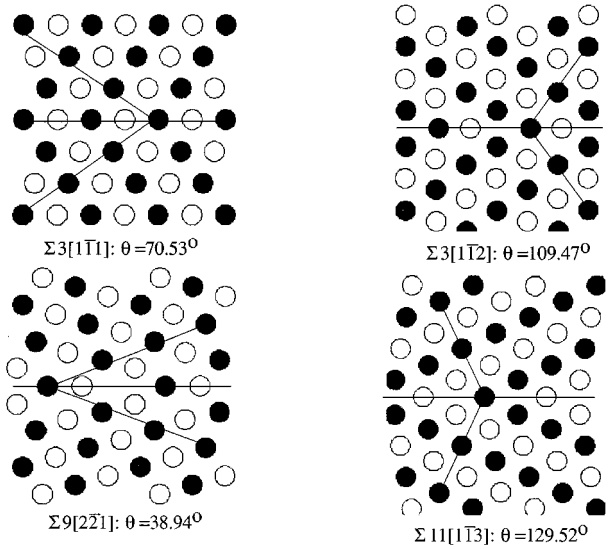

Figure 2 Equilibrium structures of selected tilt CSL grain boundaries about [1 1 0] axis of aluminum.

layers, which have been projected in a plane normal to z = [1 1 0] direction. It was observed that during the simulation process, most of the atomic movement occurs near the grain boundary plane (in the relaxed state) compared to the initial unrelaxed configurations. Associated with the atomic rearrangement that occurs upon minimization of the grain boundary energy is a relative displacement of grains in the direction perpendicular to the GB plane, Δy^* (see Fig. 1). Δy^* is one measure of the GB expansion or excess volume per unit GB area [23]. This measurement, if made far away from the GB, is not sensitive to the GB strain field, which decays away from the boundary as ye^{-y} [23], where y is the distance from GB. Table I shows a measure of the GB expansion in the relative y displacement of two atomic planes closest to the GB (i.e., the pair of planes with the largest spacing after relaxation). It is seen that the local grain boundary expansion ($\Delta y^* > 0$) is apparent for all the boundaries. It is also seen from the data that the lower Δy^* in general corresponds to a lower GB energy configuration. The equilibrium configurations shown in Fig. 2 were compared to other available computational and experimental results. The key aspect to be compared is the micro-facet structural details near the boundary, which includes the relative positions of atoms in the boundary and neighboring planes. The present results for two of the CSL structures $\Sigma 9(2\,\bar{2}\,1)$ and $\Sigma 11(1\,\bar{1}\,3)$ agree well with the experimentally observed tilt boundaries using high-resolution transmission electron microscopy (HRTEM) [7, 11, 15].

The distribution of energy across the equilibrium grain boundaries was computed next. Fig. 3 shows the energy associated with atoms as a function of distance from the grain boundary plane (x-axis zero being at the grain boundary). The energy increases as the grain boundary is approached from either side of the bicrystal. There is significant variation in the energy levels for the different boundaries considered. The width of the grain boundary can be defined when the energy of atoms equals to the value of energy in a perfect crystal (−3.58 eV for aluminum). By this definition, the width of grain boundaries varies with different boundary structures (see Fig. 3), from a maximum 10 Å to almost zero in $\Sigma 3(1\bar{1}1)$ structure.

The energy of the individual atoms (plotted in Fig. 3) can be used in the evaluation of grain boundary energy, which is equal to the energy of atoms within the width of the grain boundary in the defective system less than that for the perfect crystal, divided by the area of the grain boundary plane. Fig. 4a shows the grain boundary energy (E_{gb}) for all the tilt grain boundaries studied in this work, plotted as a function of the misorientation angle θ. As can be seen from the plot, three energy cusps for "special" angles were observed in this work, which correspond to three twin boundaries: $\Sigma 3(1\bar{1}1)$, $\Sigma 3(1\,\bar{1}\,2)$, and $\Sigma 11(1\bar{1}3)$.

Our simulation result is reasonably consistent with the experimental result conducted by Otsuki and Mizuno [22], as shown in Fig. 4b. Comparing these two sets of results, in addition to the excellent agreement of the shape of the energy vs. misorientation plots, the absolute values are also in a close range. Wolf [2, 13] and Hasson *et al.* [5] have conducted similar grain boundary simulations for copper and aluminum using pair potentials. However, they only observed energy cusps for the $\Sigma 3(1\,\bar{1}\,1)$ and $\Sigma 11(1\,1\,3)$ orientations, but not for the $\Sigma 3(1\,1\,2)$ orientation. Because $\Sigma 3(1\,1\,2)$ is also a twin boundary, it is reasonable to expect the $\Sigma 3(1\,1\,2)$ boundary to be also a low-energy defect. The observation of the new low-energy configuration $\Sigma 3(1\,1\,2)$ can be ascribed to the use of EAM potentials in this work compared to the pair potentials used in the earlier works. In the EAM calculations, the configuration energy is composed of a simple pair interaction term plus an "embedding" function, which specifies the dependence of energy on local coordination. The ability to treat deviations in local coordination has been shown to be crucial in obtaining reasonable agreement with the relaxation at interfaces and free surfaces. Thus, atoms interacting across the interface experience an electron density different from that of atoms interacting with each other on the same side of the interface. This intrinsically anisotropic character of the atoms near the interface is not taken into account by any pair potential. In general, the choice of interatomic potentials has less effect on grain boundary structures than on grain boundary energies [2, 11].

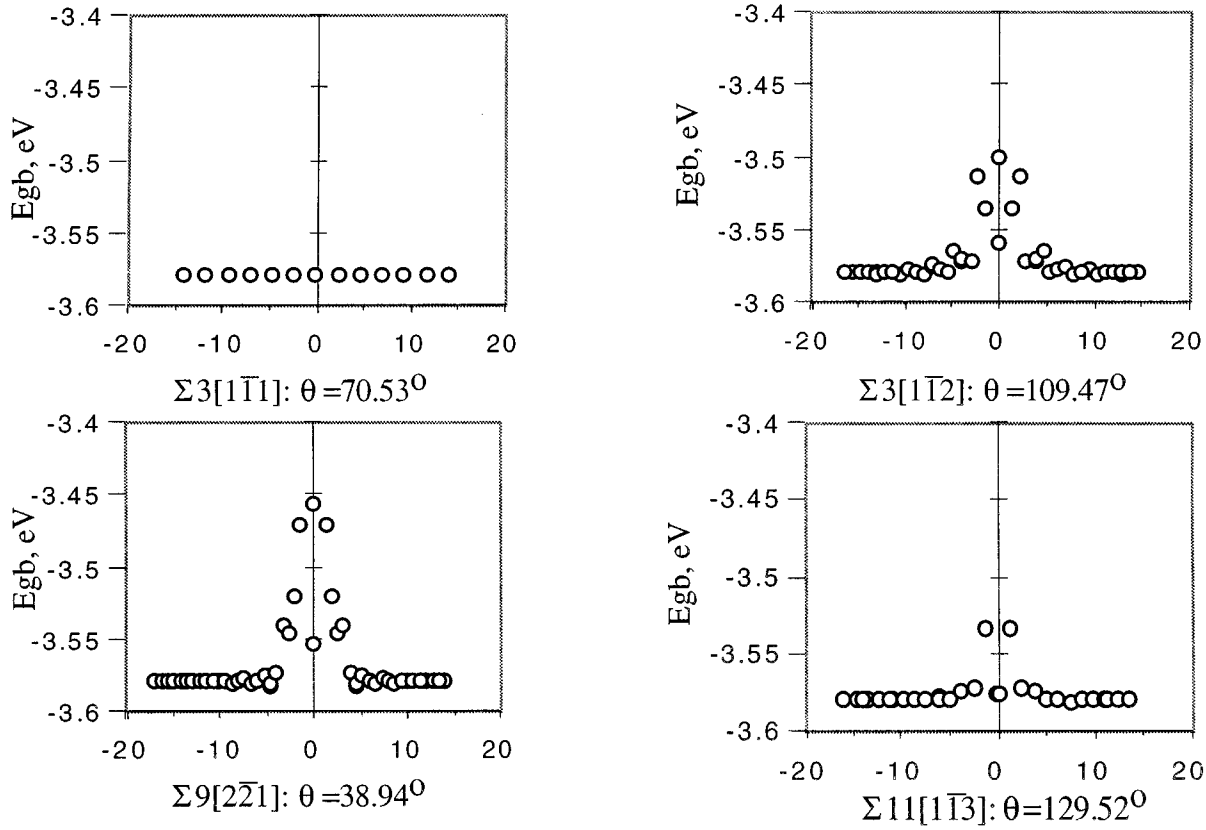

Figure 3 Energy distribution in equilibrium structures of tilt CSL grain boundaries.

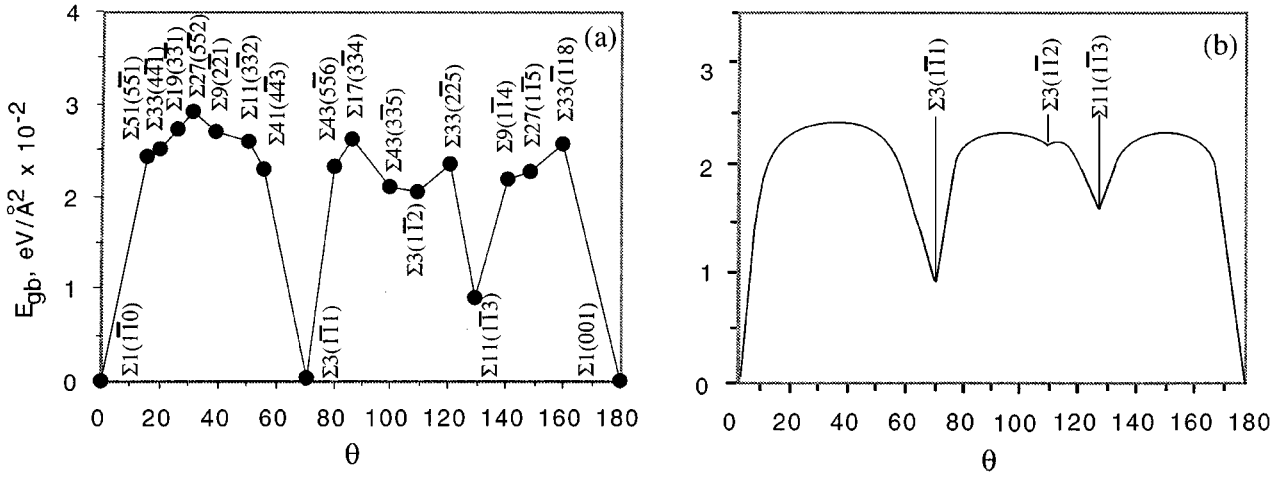

Figure 4 (a) Calculated grain boundary energy, E_{gb} of tilt CSL grain boundaries about [1 1 0] in aluminum as a function of misorientation angle, θ; (b) corresponding experimental results [24].

3. Grain boundary sliding and migration

Molecular statics/dynamics simulation was next performed to study grain boundary mobility under applied displacement and forces, as shown in Fig. 5. The computational crystal composed of about 5000 atoms with approximately 35 atomic layers (in y-direction) in each grain. In order to eliminate the effect of free surfaces associated with the grain boundary plane during the grain boundary sliding, periodic boundary conditions were applied in plane of the interface (i.e., x- and z-directions in this work). When applying displacement, specified levels of incremental displacements were applied to each of the atoms in the top grain, and all the atoms in the bottom grain remain free. It is adequate to use free-surface boundary conditions in the grain boundary normal direction (y-direction). When forces are applied on all the atoms in the top grain, it simulates the actual motion of the top grain as a single unit over the bottom grain. In this case, it is necessary to restrict the motion along the two surfaces in y-direction, which is achieved by setting y-displacement to zero on the atoms near the upper surface (four outermost layers in y-direction) and fixing the bottom surface (four outermost layers in y-direction). These boundary conditions ensure that the molecular dynamics simulation was performed at a constant volume condition. As will be evident later, application of displacements and force yield different responses; displacement causes “pure”

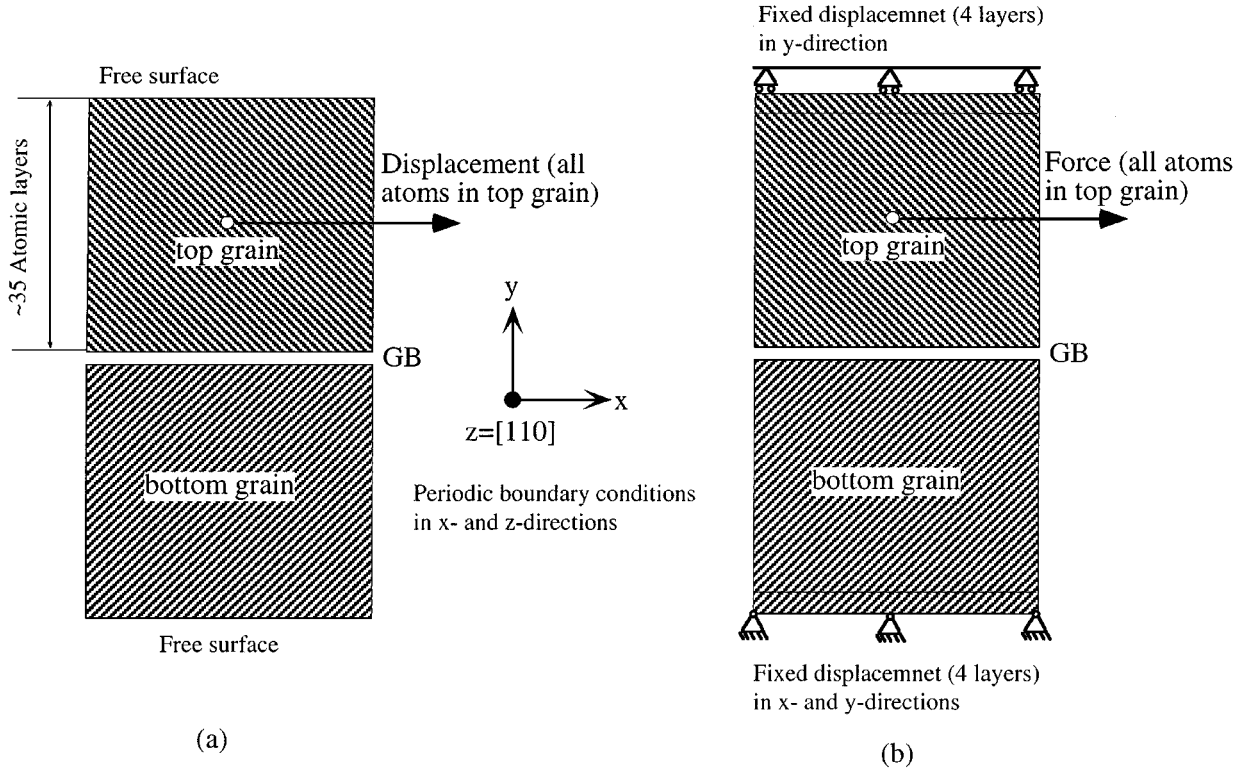

Figure 5 Boundary conditions of the computational crystals under (a) applied displacement and (b) applied force.

GBS, whereas force induces sliding and migration. For brevity, only the results for $\Sigma 3(111)$ and $\Sigma 9(2\,\bar{2}\,1)$ are presented and discussed below.

3.1. Applied displacement

Under the applied displacement conditions, grain boundary migration (atomic movement in the direction normal to the applied displacement direction) was physically constrained. Thus, application of displacement increments simulate a "pure" GBS process. Each increment is followed by a complete relaxation (energy minimization) of the boundary structure. Because the CSL grain boundary structure studied in this work can be obtained by repeating the CSL cell in x- and z-directions, the structure with a displacement of a_{CSL} (a_{CSL} is the lattice parameter of the CSL cell in x-direction) is equivalent to the initial undisplaced structure under the periodic conditions described above. Therefore, the total displacement in each case is limited to the value of a_{CSL} for the given grain boundary. The increments (described in percentage of a_{CSL}) are selected to be small enough (2.5%a_{CSL}) to capture all the energy jumps. After each increment, the configuration is relaxed to its local equilibrium state and the grain boundary energy is computed. The grain boundary energy profile associated with the GBS process then provides the tool necessary to predict the grain boundary mobility. Figs 6 and 7 give such results for two typical grain boundaries: a twin boundary $\Sigma 3(1\bar{1}1)$ and a $\Sigma 9(2\,\bar{2}\,1)$ boundary.

Fig. 6 shows the energy profile of "pure" GBS process in $\Sigma 3(111)$ twin structure. Fig. 6 shows that there are two energy peaks and a energy valley between them. The first peak occurs when the shear displacement is about 17% a_{CSL} (case II in the figure), where the atoms represented by open (and filled) circles are directly above the filled (and open) circles across the boundary. This configuration corresponds to a set of atoms in adjacent (1 1 0) planes displaced by d_{220} amount in the z-direction. When the shear displacement is about 66% a_{CSL} (case IV in the figure), the atoms across the interface plane are at positions directly facing each other, and furthermore, these atoms facing each other are in the same (1 1 0) plane. It can be seen that open circle is the exactly above open circle (filled circle is exactly above filled circle). In case IV, the separation distances between atoms across the boundary is the smallest, and the corresponding energy value is the largest as seen in the energy plot. Between these two high energy states (cases II and IV), there is an energy valley at the 33% a_{CSL} shear displacement (see case III). The atomic arrangement at this displacement forms a twin structure equivalent to the initial structure. Although the interface of the twin has shifted (from AA to BB) with d_{111} amount in the y-direction, this boundary has an energy equal to the initial twin structure. It is interesting to notice that though "pure" GBS is being simulated, one-layer of migration was observed for a specific displacement, as shown in case III. This demonstrates the geometrical necessity of coupling between migration and sliding. This aspect will be discussed in detail in section 3.3.

In the case of $\Sigma 9(2\,\bar{2}\,1)$ boundary, shown in Fig. 7, the energy barrier in the initial phase of the GBS process (from 0 to 52% a_{CSL}) is relatively small. A big energy jump appears when the atoms across the boundary face each other (52–58% a_{CSL} shear displacements, case II). After the short jump, the GBS process proceeds easily. The atomic configuration corresponding to case II represents the worst stability of the grain

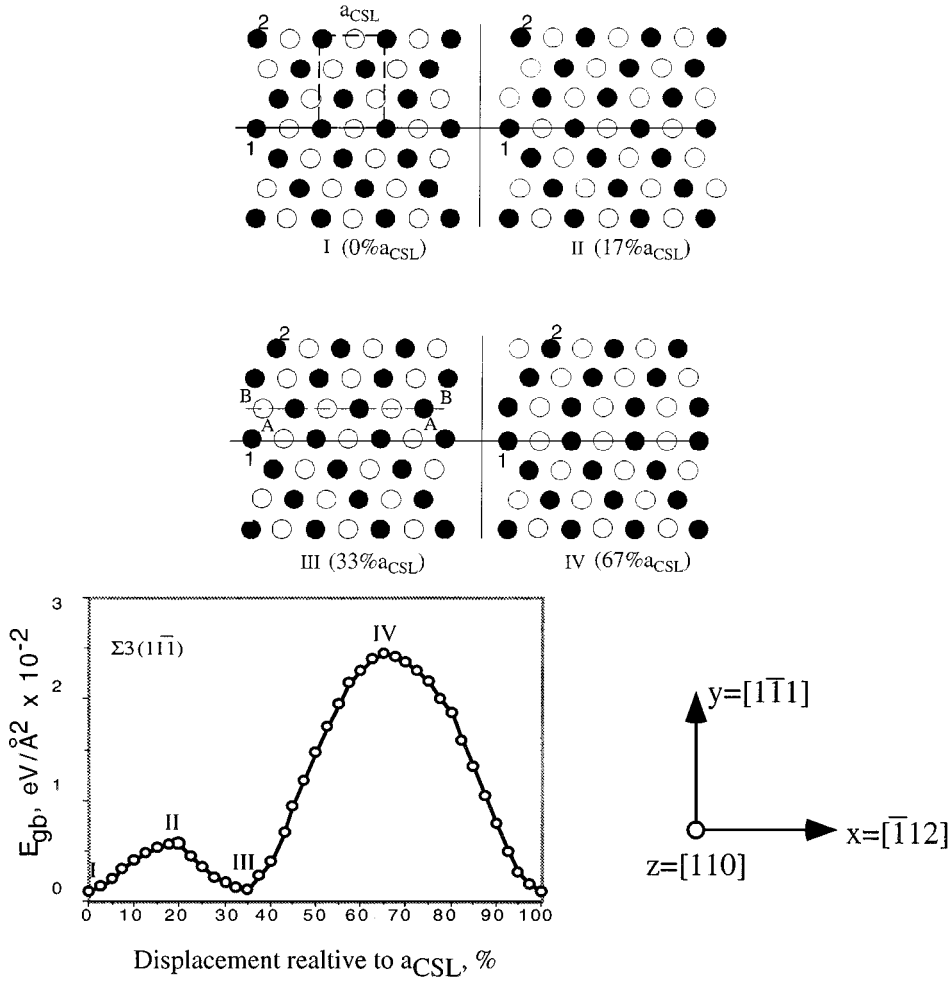

Figure 6 Energy evolutions during GBS process of $\Sigma 3[1\bar{1}1]$ tilt CSL boundary.

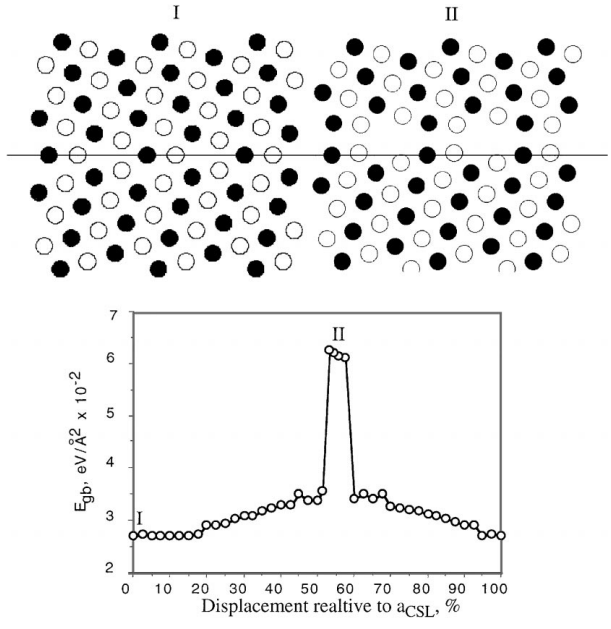

Figure 7 Energy evolutions during GBS process of $\Sigma 9(2\,2\,\bar{1})$ tilt CSL boundary.

boundary structure. Atoms across the interface plane in this case are at positions directly facing each other and in the same (1 1 0) plane (open circle is the exactly above open circle, and filled circle is exactly above filled circle). When comparing the GBS process in $\Sigma 9(2\,2\,\bar{1})$ boundary with that in $\Sigma 3(1\bar{1}1)$ boundary, although the magnitude, width, and distribution of the energy barriers are quite different for the two GB structures, the energy diagrams during the GBS show a general pattern: (1) The initial CSL structure and the final displaced structure with 100%a_{CSL} displacement have the lowest energies, any structure between them have equal or high energies. The GBS process destroys the CSL arrangement of the initial equilibrium grain boundary structure and increases the grain boundary energy; and (2) energy jumps (energy barriers) occur when the displacement is such that some atoms in the two adjacent (h k l) planes across the grain boundary interface (one in each of the bicrystals) are directly above (or below) each other. As declared earlier, the (h k l) interplanar spacing (all less than $0.6a_e$) is substantially less than the nearest-neighbor distance in the perfect crystal ($0.707a_e$ in FCC structure); all atoms facing each other across the grain boundary interface repel each other. In the configurations with energy peaks, some atoms across the interface are too close to each other, and hence, have very high energies.

3.2. Applied forces

To study grain boundary mobility under applied force conditions, a force of specific value (ranging from 0.01 to 0.04 eV/Å) is applied in the x direction (to the right)

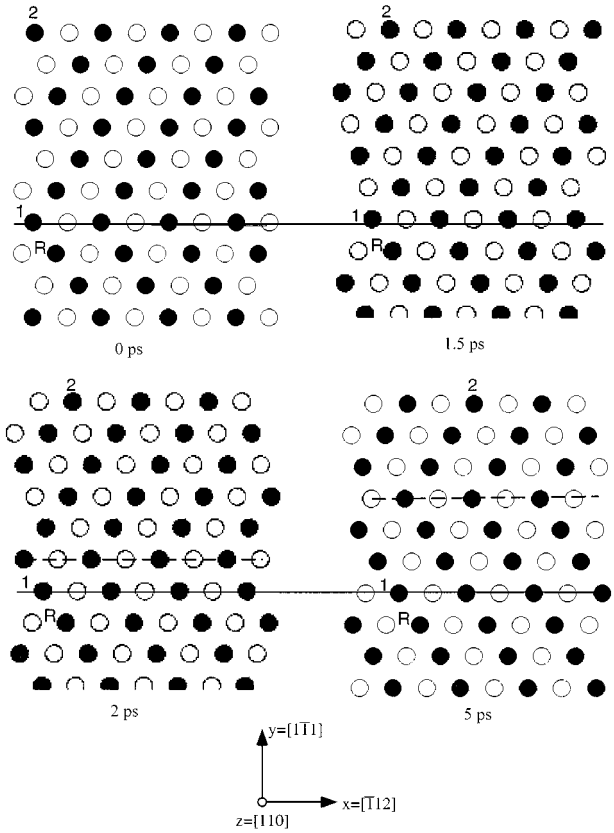

Figure 8 Evolution of $\Sigma 3[1\bar{1}1]$ grain boundary structure under applied force.

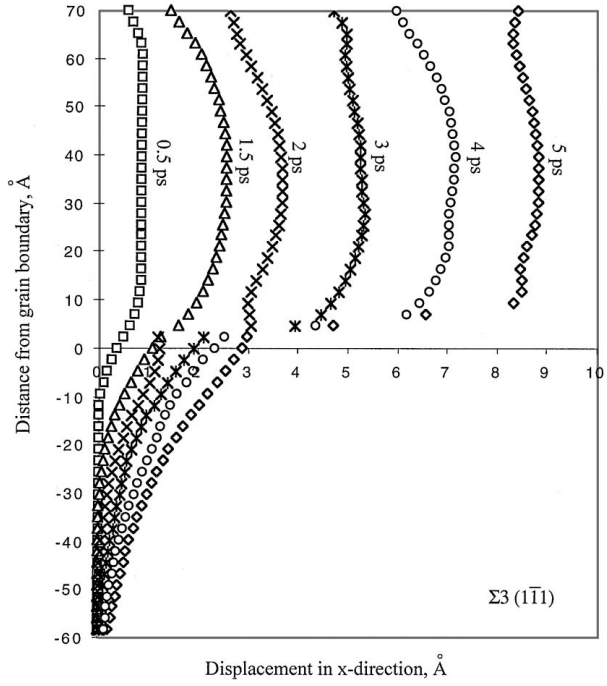

Figure 9 Relative displacement in x-direction as a function of time.

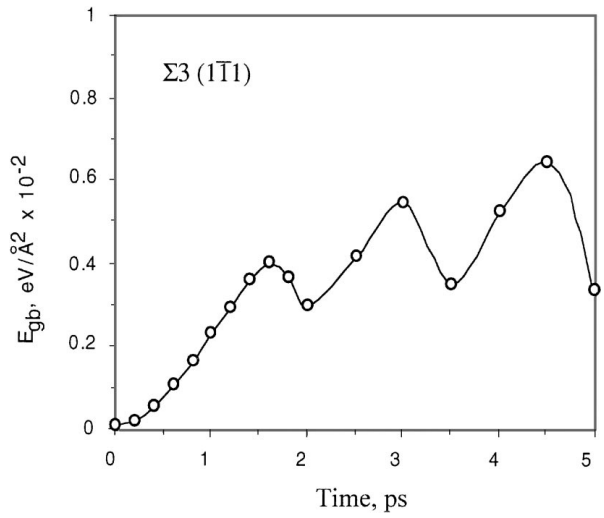

Figure 10 Grain boundary energy change during the simulation.

on the atoms in upper half of the bicrystals. Fig. 8 shows the simulation result for $\Sigma 3(1\,1\,1)$ twin boundary. It can be seen that applied forces cause relative motion across the boundary between two grains, leading to GB sliding. This is evident from the relative position of atoms numbered R, 1 and 2. Atom R is in the bottom grain, atom 1 is on the GB, and atom 2 in the top grain away from the boundary. It should be noted that the periodic boundary condition fills in new atoms from the left as atoms slide to the right of the computational crystal. Apart from sliding, GB also migrates, that is, the interface that forms the boundary between two grains moves perpendicular (in y-direction) to the original GB plane. Such motion can be observed at 2 ps where the GB interface has moved one atomic layer (dotted line), and by about 3 atomic layers at 5 ps (see Fig. 8).

To get a quantitative understanding of the grain boundary sliding, the average x-displacement of atoms lying along y-axis are plotted in Fig. 9. As seen from this figure, the displacement field shows a sharp discontinuity across the interface indicating relative motion of atoms across the boundary resulting in GB sliding. The figure also shows that the magnitude of GB sliding increases with time. Thus, Fig. 9 (showing sliding) and Fig. 8 (showing migration and sliding) demonstrate that sliding and migration are coupled in this system.

GB energy during the deformation process is plotted as a function of time in Fig. 10. This figure indicates that the energy continuously varies with a few peaks and valleys, which corresponds to the evolving GB structure during the deformation. For example, a peak is observed at 1.5 ps because the atoms in the layer just above the interface directly face the atoms in the interface (see also Fig. 8 at 1.5 ps). In this case, the interplanar spacing in y-direction ($0.577a$) is substantially less than the equilibrium nearest-neighbor distance in the perfect crystal ($0.707a$ in FCC structure). This occurs because the atoms facing each other across the grain boundary are too close to each other, and hence, repel. Several energy valleys (at 2, 3.5, and 5 ps) correspond to new twin configurations (with different interface positions). However, as shown in Fig. 10, their energies are still much higher than the energy of stress-free twin structure (0 ps).

A similar process was observed in $\Sigma 9$ grain boundary, as shown in Fig. 11. Due to its incoherent interface and higher grain boundary energy, the initial grain boundary sliding appears earlier than that of $\Sigma 3$ case. The migration distance at each step is shorter due to the smaller d_{221} interplanar spacing in

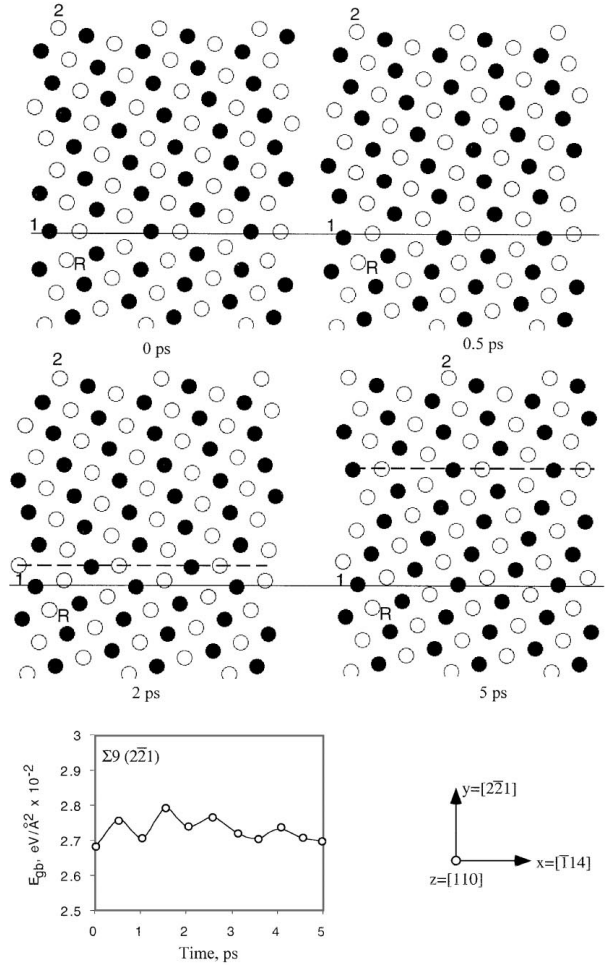

Figure 11 Evolution of $\Sigma 9[2\,\bar{2}\,1]$ grain boundary structure and energy under applied force.

y-direction of this boundary. The sliding occurs first (Fig. 11, 0.5 ps). When the sliding displacement in the x-direction reaches d_{114}, the grain boundary interface migrates one atomic layer (d_{221}) up along the y direction (Fig. 11, 1 ps). Thus, coupled sliding and migration process appears very similar to that in $\Sigma 3$ case. However, as also shown in Fig. 11, the change in grain boundary energy during the simulation process is very different. In contrast to $\Sigma 3$ case, the energy barrier in this case is much smaller (about 0.1×10^{-2} eV/Å^2). It is, therefore, to be expected that the GBS and GB migration are much easier in the $\Sigma 9$ (high energy GB) than that of $\Sigma 3$ (low energy twin GB).

3.3. Comparison between applied displacement and applied stress conditions

From the foregoing discussions, it is clear that in STGB, when forces are applied, GB sliding is always accompanied by grain boundary migration, and they are proportional to each other. A similar coupled process has been observed by Ashby [25] based on the bubble raft model and by Bishop *et al.* [17, 18] based on purely geometric considerations for STGB. This coupling process is of practical importance, and hence examined from geometry, energy, and stress field considerations in the following sections.

3.3.1. Geometrical consideration of coupled sliding and migration

For understanding the geometrical aspects of coupling migration with sliding, it is easier to analyze the motion in terms of displacement shift completed (DSC) lattice vectors. Translations of one crystal with respect to another by a DSC lattice vector (the finer mesh in Fig. 1) restore the coincidence pattern, although the coincidence sites will shift to a different location. This GB shift corresponds to the GB migration. For example, $\Sigma 3(1\bar{1}1)$ boundary has the following DSC lattice parameters: $a_{DSC} = 1/3a_{CSL} = d_{112}$, $b_{DSC} = 1/3b_{CSL} = d_{111}$, and $c_{DSC} = c_{DSC} = d_{110}$. When the relative translation of the crystals is a_{DSC} in the x-direction, the boundary migrates by b_{DSC} in the y-direction. The CSL structure is reestablished one unit away in the y-direction. The ratio (R) of migration distance (M) to sliding displacement (U) is

$$R = \frac{M}{U} = \frac{b_{DSC}}{a_{DSC}} = \epsilon \tan \frac{\theta}{2} \tag{1}$$

Here the misorientation angle θ is defined as the angle between the two [0 0 1] directions of each of the bicrystals (see Fig. 1), ϵ is a integer whose value depends on the details of geometry. Equation 1 is valid for all symmetric tilt boundaries as pointed out by Ashby [25]. It should be noted that this geometric argument is truly valid only for STGB [18]. However, it does not preclude coupling to occur in other types of boundaries.

In the applied displacement case, after a displacement of a_{DSC} in the top grain, GB moves by b_{DSC} (see III in Fig. 6). However, when the displacement is further applied (including layer BB), GB interface moves back to the original position (line AA). When forces are applied, GB migrates upwards continuously after each a_{DSC}. This difference will be more clear from energy consideration discussed below.

3.3.2. Energetic consideration of coupled sliding and migration

The energy necessary to couple sliding and migration can be seen readily by comparing the grain boundary energy profiles shown in Figs 6 and 10 for $\Sigma 3(1\bar{1}1)$ boundary and Figs 7 and 11 for $\Sigma 9(2\,\bar{2}\,1)$ boundary. Let us first consider $\Sigma 3(1\bar{1}1)$, i.e. Figs 6 and 10. The initial energy profiles in both cases (0–40%a_{CSL} displacement in Fig. 6 and 0–2 ps in Fig. 10) are similar. This indicates that the deformation processes are same at this stage regardless of whether force or displacement is applied. Also, when the structures are examined, it is seen that the grain boundary shown in Fig. 10 only experienced GBS without migration similar to Fig. 6, leading to the two energy profiles being very similar. However, the energy profiles are very different in the subsequent stages. The results shown in Fig. 10 (applied force) confirm that when sliding is accompanied by migration, boundary structure never passes through a highly perturbed configuration (e.g., Case IV in Fig. 6). By virtue of the coupling between sliding and migration, the energy barrier for grain boundary motion is

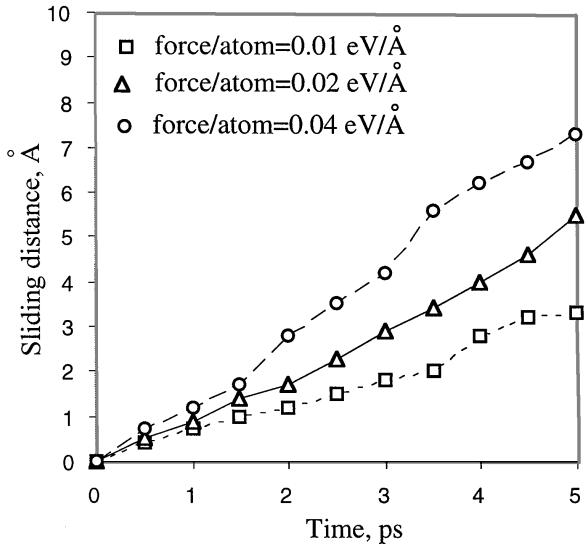

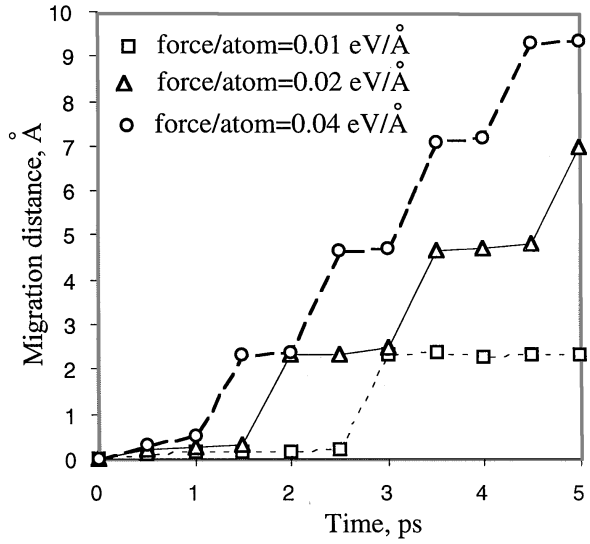

Figure 12 The displacement fields in $\Sigma 3(1\,\bar{1}\,1)$ grain boundary.

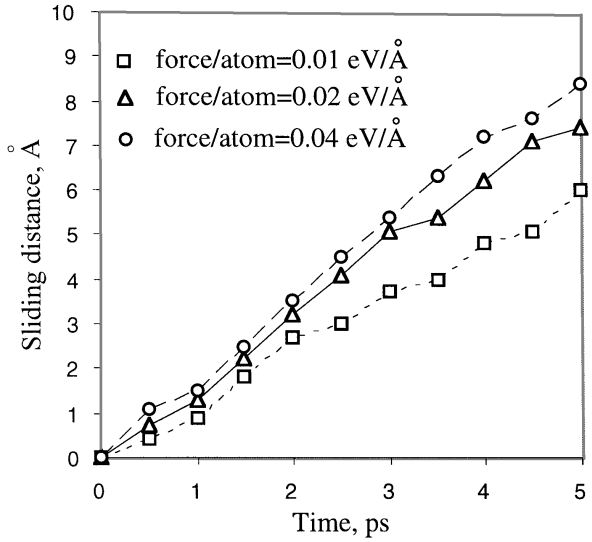

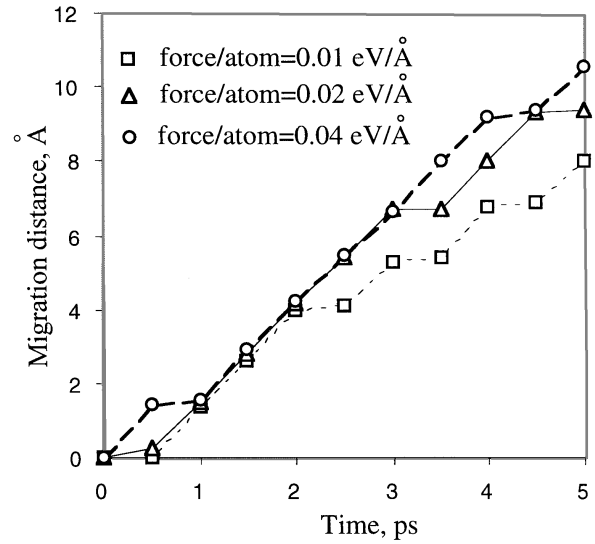

Figure 13 The displacement fields in $\Sigma 9\,(2\,\bar{2}\,1)$ grain boundary.

greatly reduced from about 2.5×10^{-2} eV/Å^2 in Fig. 6 to 0.5×10^{-2} eV/Å^2 in Fig. 10. Simulation of a perfect crystal with the same orientation as shown in Fig. 6 indicated that an peak energy of 9.3×10^{-2} eV/Å^2 is required to displace one portion of the crystal against the other. This indicates that the high energy peak in Fig. 6 (applied displacement) corresponds to sliding in a less defect region (line AA) rather than along the new GB interface (line BB). The effect of coupled sliding and migration on energy is more obvious in $\Sigma 9(2\,\bar{2}\,1)$ boundary, where the energy barrier is dropped from about 3.5×10^{-2} eV/Å^2 in Fig. 7 to 0.1×10^{-2} eV/Å^2 in Fig. 11. These results indicate that the high energy state during the pure GBS (e.g., Fig. 9 II) is never reached in the coupled GBS and migration process.

3.3.3. Displacement and stress fields of coupled sliding and migration

In the applied force conditions, both the sliding and migration displacement fields are directly related to the magnitude of applied force, and are also a function of the grain boundary structures themselves. Fig. 12 shows the displacement field changes under three levels of applied forces for $\Sigma 3(1\bar{1}1)$, and Fig. 13 shows the data for $\Sigma 9(2\,\bar{2}\,1)$. The sliding displacements were computed from the relative position of two grains across the interface (see Fig. 9). The migration displacements were the difference in y-direction between the positions of new interface and the original equilibrium position of the interface. As can be seen from these two figures, as the applied force increases (from 0.01 to 0.04 eV/Å), both the sliding and migration displacements increase but in quite a different fashion. Sliding displacements increase monotonically with time. Migration displacement increases in steps, each step indicating that the interface has migrated one atomic layer along the y-direction. However, the sliding and migration are coupled and proportional, and anything that inhibits sliding also inhibits migration.

It is also noted from Figs 12 and 13 that the structure of the grain boundary has great influence on GBS. To understand this effect, the GBS displacement for four different grain boundaries with increasing energy levels under same total applied force per unit volume

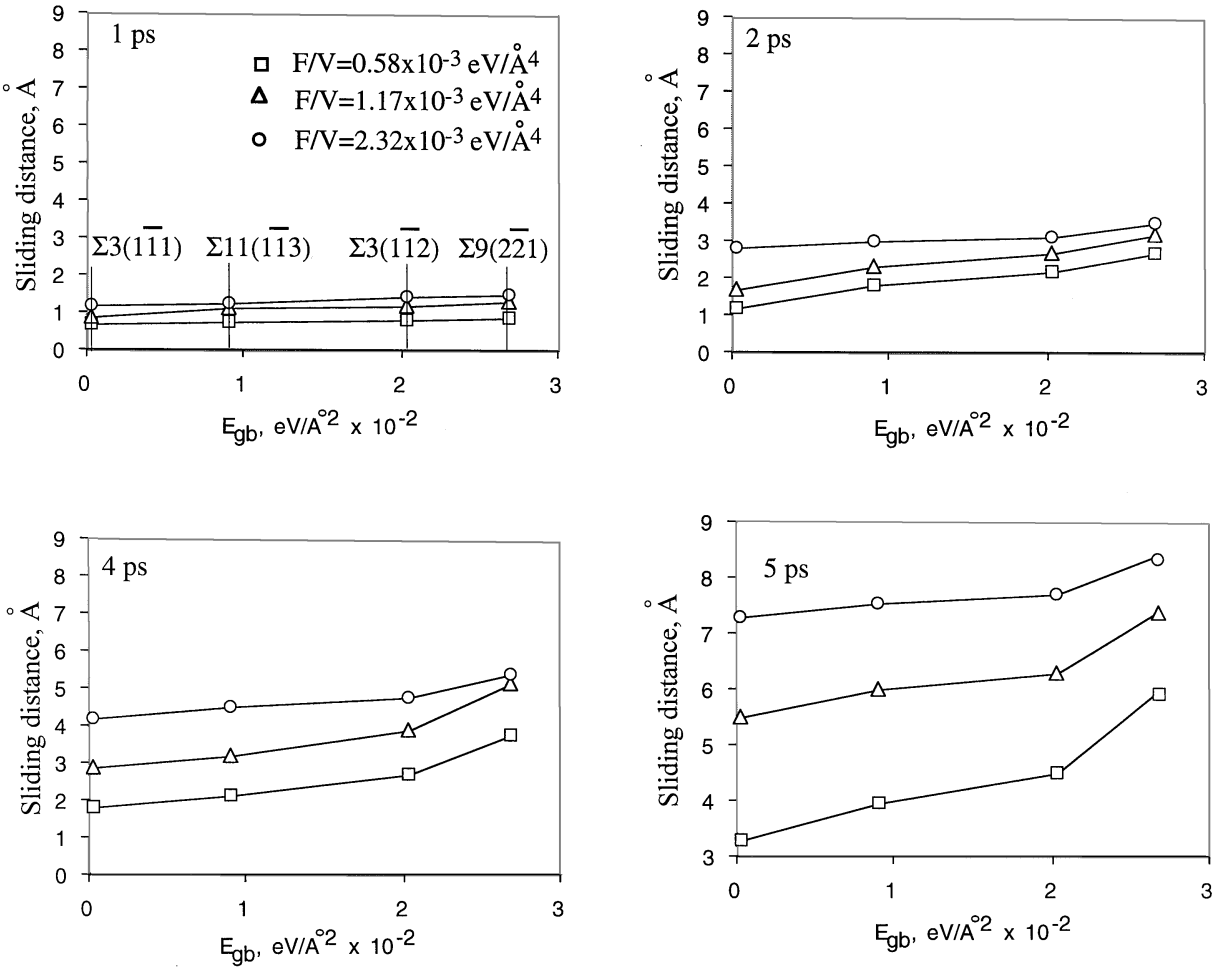

Figure 14 Grain boundary energy effect on GBS (F/V is the total force per unit volume).

was examined. The consolidated displacement (sliding and migration) vs. GB energy response are shown in Fig. 14. It is clearly seen that GBS displacement is proportional to the grain boundary energy associated with a given structure. For example, at 5 ps, $\Sigma 3(111)$ boundary slides 3.3, 5.5, and 7.2 angstroms at applied forces 0.58, 1.17, and 2.32 (in unit of $\pm 10^{-3}$ eV/Å^4 per volume) respectively, while $\Sigma 9(2\,\bar{2}\,1)$ slides 5.9, 7.4, and 8.5 angstroms under the same levels of applied forces. These results are consistent with the energy profile during the simulation (Figs 10 and 11), that is, higher energy boundary such as $\Sigma 9(2\,\bar{2}\,1)$ has lower energy barriers for grain boundary movements and hence produces more sliding and migration displacements. Although it is tempting to write that grain boundary displacement u_d and migration u_m are proportional to GB energy E_{gb}, we need to understand energy and stress distribution across the GB plane in three dimensions, before we can formulate the realationship.

In order to analyze the internal stress fields resulting from the applied force and applied displacement, the $\alpha\beta$ components of the local stress tensor $\sigma^i_{\alpha\beta}$ associated atom i is calculated as follows:

$$\sigma^i_{\alpha\beta} = \frac{1}{V}\sum_{j,i\neq j}\left(F'_i\rho'^{\alpha}_j + F'_j\rho'^{\alpha}_i + \phi'_{ij}\right)\frac{r^{\alpha}_{ij}r^{\beta}_{ij}}{r_{ij}}$$

$$(\alpha, \beta = 1, 2, 3) \quad (2)$$

where V is the volume of the computational crystal, r^{α}_{ij} is the α^{th} component of the relative position vector of atom i and j; and F'_i, ρ'_j, and ϕ' are the derivations of the EAM functions [12]. For brevity, only the results of $\Sigma 3(111)$ are given and discussed below.

Fig. 15 shows the local stress field near the grain boundary (σ_{11}) for the atomic configurations under applied displacement (Fig. 6, case IV) and applied force (Fig. 8, 5 ps). The lengths of the arrows in Fig. 15 initiate at the atomic positions and scale with the magnitude of the local stresses, and the direction of the arrow shows the sign of the local stresses. Note that due to the use of the periodic boundary conditions, the

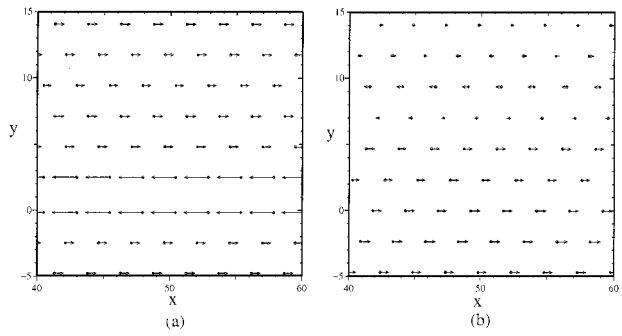

Figure 15 Local stress (σ_{11}) distribution in $\Sigma 3$ $(1\bar{1}1)$ boundary under (a) applied displacement (case IV in Figure 6) and (b) applied force (5 ps in Figure 8).

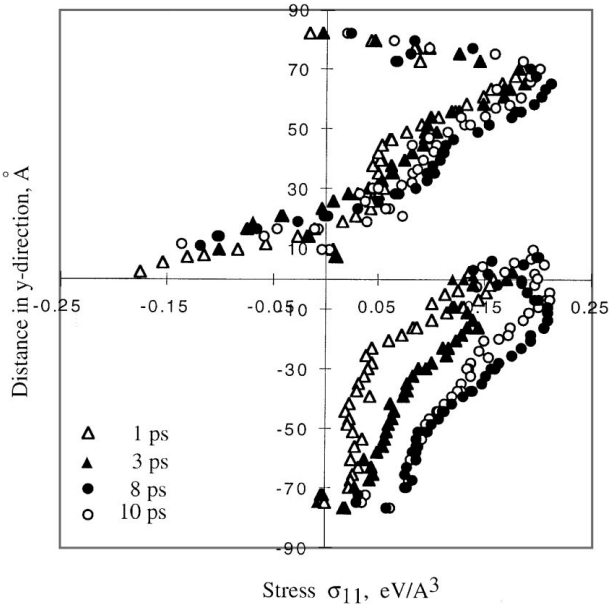

Figure 16 Stress (σ_{11}) fields in $\Sigma 3\,(1\bar{1}1)$ grain boundary under applied stress (0.04 eV/Å).

stresses are same for all the atoms that reside in the same atomic layer in the y-direction. In the applied displacement case (Fig. 15a), the stresses are much higher in the grain boundary region. In the applied force case (Fig. 15b), the stresses are more uniformally distributed around the GB interface. When displacements are applied (Fig. 15a), σ_{11} changes direction across the interface indicating the presence of large shear stresses necessary for force equilibrium. This shear stress opposes GBS motion.

Finally, to understand the relations between the internal stress and external applied force, the overall stress distribution for the whole computational crystal was computed. Fig. 16 shows the results of $\Sigma 3(111)$ at the applied force of 0.04 eV/Å. As the simulation proceeded, the internal stresses built up and increased gradually. The σ_{11} stress discontinuity was found in the region close to the interface, indicating the shear resistance to the grain boundary movements. The integration of the stress (times the distance from the interface) across the whole computational crystal was calculated and normalized to the internal force to one atom. This normalized force has values (in unit of eV/Å) of 0.0027 (at 1 ps), 0.0031 (at 2 ps), 0.0091 (at 3 ps), 0.015 (at 4 ps), 0.028 (at 5 ps), 0.031 (at 8 ps), and 0.029 (at 10 ps) at corresponding simulation times. It is seen that as the simulation time increases, the integration of the stress (i.e., the force) increases towards to the value of applied force (0.04 eV/Å). Lack of static force balance indicates transient conditioning in which a state of dynamic equilibrium is present. The external forces do match at 8 ps, when the internal stress distribution induced resistive forces equal the applied force. Thus, it is clear from the stress distribution that the relative displacement is restricted to a small region around the interface and is proportional to the energy associated with the GB interface.

4. Conclusion

Interatomic potentials using Embedded Atom Method (EAM) are used in conjunction with molecular statics and dynamics calculations to study the sliding and migration of (1 1 0) symmetric tilt grain boundaries (STGB) in aluminum, under both applied displacement and force conditions. Three low energy configurations (corresponding to $\Sigma 3(1\bar{1}1)$, $\Sigma 3(1\,1\,\bar{2})$ and $\Sigma 11(1\,1\,\bar{3})$ twin structures) are found in the [1 1 0] STGB structures when grain boundary energies at 0 K are computed as a function of grain misorientation angle. Application of displacement increments to atoms on one of the grains in a grain pair results in the simulation of "pure" GBS (without migration). In contrast, when forces are applied to the same atoms, the energy barriers are reduced due to the fact that grain boundary sliding of STGB is always coupled with migration. The propensity for "pure" GBS is evaluated by computing the energy associated with incremental equilibrium configurations during the sliding process, and the magnitude of the energy barriers is found to be much higher than that with migration. Thus, the study clearly shows that in these special grain boundaries (STGBs), migration is coupled with sliding during GBS. It is seen that when the free energy in the grain boundary decreases (more specialized boundaries approaching twin boundaries), the boundary offers more resistance to sliding and, consequently, migration. The computational results show that the amount of sliding and migration is proportional to the applied force levels, grain boundary energy, and the time period of deformation process. The results indicate that if we can engineer grain boundary (and alter the associated energy values), then the GB energy should be increased to decrease deformation rate (e.g., creep resistance), and decreased to promote sliding (e.g., superplasticity).

Acknowledgements

The authors wish to acknowledge Army Research Office and project monitors, Drs. Andrew Crowson and Wilbur Simmons, for providing partial financial assistance in support of the project.

References

1. T. R. MCNELLY and M. E. MCMAHON, *Mater. Trans. A.* **27** (1996) 2252.
2. D. WOLF, *Acta Metall.* **32** (1984) 245.
3. Y. OH and V. VITEK, *Acta Metall.* **34** (1986) 1491.
4. D. WOLF, *Acta Metall.* **32** (1984) 245.
5. G. HASSON, J.-Y. BOOS, I. HERBEUVAL, M. BISCONDI and C. GOUX, *Surf. Sci.* **31** (1972) 115.
6. G. J. WANG, A. P. SUTTON and V. VITEK, *Acta metall.* **32** (1994) 1093.
7. U. DAHMEN, C. J. D. HETHERINGTON, M. A. O'KEEFE, K. H. WESTMACOTT, M. J. MILLS, M. S. DAW and V. VITEK, *Phil. Mag. Letters* **62** (1990) 327.
8. A. P. SUTTON and R. W. BALLUFFI, *Acta Metall.* **35** (1987) 2177.
9. J. WANG and V. VITEK, *Acta Metall.* **34** (1986) 951.
10. A. P. SUTTON and R. W. BALLUFFI, "Interface in Crystalline Materials" (Oxford University Press, 1995).
11. M. S. DAW, S. F. FOILES and M. I. BASKES, *Mater. Sci. Reports* **9** (1993) 251.
12. P. DANG and M. GRUJICIC, *Mater. Sci. and Eng.* **4** (1996) 123.

13. D. WOLF, *J. Appl. Phys.* **68** (1990) 3221.
14. *Idem, ibid.* **69** (1990) 185.
15. M. J. MILLS, *Mater. Sci. Eng.* **A166** (1993) 35.
16. J. M. RICKMAN, S. R. FILLET, D. WOLF, D. L. WOODRASKA and S. YIP, *J. Mater. Res.* **6** (1991) 2291.
17. G. H. BISHOP, JR, R. J. HARRISON, T. KWOK and S. YIP, *J. Appl. Phys.* **53** (1982) 5609.
18. *Idem ibid.* **53** (1982) 5596.
19. C. MOLTENI, G. P. FRANCIS, M. C. PAYNE and V. HEINE, *Mater. Sci. Eng.* **B37** (1996) 121.
20. D. J. OH and R. A. JOHNSON, "Atomistic Simulations of Material: Beyond Pair Potentials," edited by V. Vitek and D. J. Srolovitz (Plenum Press, 1989, p. 223).
21. S. F. FOILES, private communication, 1996.
22. G. PALUMBO, E. M. LEHOCKEY and P. LIN, *JOM* **50** (1998) 40.
23. C. P. CHEN, D. J. SROLOVITZ and A. F. VOLTER, *J. Mater. Res.* **4** (1989) 62.
24. A. OTSUKI and M. MIZUNO, Proceeding Symosiam on Grain Boundary Structure and Related Phenomena (Thans. Japan Inst. Metals, Suppl. 27 1986) p. 789.
25. M. F. ASHBY, *Surf. Sci.* **31** (1972) 498.

Received 8 June
and accepted 26 August 1998